A PBPK Digital Twin of Rapamycin for Predicting Dose–Exposure Relationships, Organ Impairment Effects, and Drug–Drug Interactions

Monika Jesionek and Matthias König *

Posted Date: 6 May 2026

doi: 10.20944/preprints202605.0328.v1

Keywords: rapamycin; sirolimus; PBPK modeling; digital twin; mTOR inhibitor; drug–drug interactions; organ impairment; personalized medicine

 doi:10.20944/preprints202605.0328.v1

Article

A PBPK Digital Twin of Rapamycin for Predicting Dose–Exposure Relationships, Organ Impairment Effects, and Drug–Drug Interactions

Monika Jesionek [1] and Matthias König [2,3,4,*]

[1] Jagiellonian University Medical College, Faculty of Pharmacy, Kraków, Poland
[2] Humboldt-Universität zu Berlin, Faculty of Life Sciences, Department of Biology, Institute of Theoretical Biology, Systems Medicine of the Liver, Berlin, Germany
[3] University of Stuttgart, Institute of Structural Mechanics and Dynamics in Aerospace Engineering, Stuttgart, Germany
[4] University of Southern Denmark, Clinical Pharmacology, Pharmacy and Environmental Medicine, Department of Public Health, Denmark
* Correspondence: koenigmx@hu-berlin.de

Abstract

Sirolimus is a potent mTOR inhibitor used primarily to prevent acute rejection in transplant recipients. Its clinical management is challenging because of its narrow therapeutic index, low and highly variable oral bioavailability, and pronounced inter-individual variability driven by CYP3A4/5-mediated metabolism and P-glycoprotein efflux. Extensive partitioning into erythrocytes further complicates its disposition and necessitates therapeutic drug monitoring. Here, we developed a mechanistic whole-body physiologically based pharmacokinetic (PBPK) digital twin of rapamycin that integrates complex absorption kinetics, nonlinear distribution, and first-pass metabolism. The SBML-encoded model was calibrated and evaluated against a comprehensive library of curated clinical pharmacokinetic data, comprising studies primarily in healthy volunteers and stable renal transplant recipients. The dataset covers diverse ethnic populations, cohorts with varying degrees of renal and hepatic impairment, and individuals with relevant genetic polymorphisms. The digital twin captured overall trends in rapamycin blood concentrations across a wide range of doses and dosing regimens. Simulations showed good agreement with observed data under hepatic and renal impairment, as well as under fasted and fed conditions. Furthermore, the model reproduced the magnitude of drug–drug interactions involving potent CYP3A4 inhibitors, CYP3A4 inducers, and concomitant immunosuppressive agents. This SBML-based digital twin provides a quantitative framework for characterizing sirolimus dose dependency and the multifactorial effects of intrinsic and extrinsic factors on systemic exposure. By providing the model in a standards-based, executable format together with simulation scripts and curated pharmacokinetic datasets, this work supports independent reproduction, transparent model evaluation, and systematic reuse in accordance with FAIR principles.

Keywords: rapamycin; sirolimus; PBPK modeling; digital twin; mTOR inhibitor; drug–drug interactions; organ impairment; personalized medicine

1. Introduction

The mammalian target of rapamycin (mTOR) is a serine/threonine protein kinase that integrates signals from growth factors, nutrients, and cellular energy status to regulate cell growth, proliferation, and metabolism. mTOR inhibitors, including rapamycin and its analogues, allosterically interact with mTOR complex 1 (mTORC1; the rapamycin-sensitive complex), thereby suppressing its activity [1,2]. Rapamycin, also known as sirolimus, is a macrolide isolated from *Streptomyces hygroscopicus*. Initially investigated as an antifungal agent, rapamycin is now widely used to prevent organ transplant rejection because of its immunosuppressive properties [3,4]. It acts by binding to FKBP-12, forming a

 doi:10.20944/preprints202605.0328.v1

complex that inhibits mTORC1 and thereby suppresses T-lymphocyte activation and proliferation, a key mechanism in preventing immune-mediated graft rejection [1,5].

Rapamycin is rapidly absorbed from the gastrointestinal tract and has a long terminal half-life ($T_{1/2}$). Its oral bioavailability is relatively low because of extensive first-pass metabolism and efflux by intestinal P-glycoprotein. Once absorbed, rapamycin distributes extensively into blood cells, resulting in pronounced partitioning between plasma and whole blood. Metabolism occurs primarily via CYP3A4 in the liver and intestine, after which rapamycin is converted to metabolites that are eliminated mainly in faeces [6–8]. Following oral administration, rapamycin exposure shows substantial inter-individual variability, driven by its lipophilic properties, limited gastrointestinal stability, patient-specific physiology, genotype, food intake, and co-administered drugs. Consequently, patients may differ markedly in systemic exposure even after receiving the same dose [7,9].

The complexity of rapamycin disposition, together with the incomplete understanding of factors underlying its pharmacokinetic variability, constrains the predictive power of empirical models and limits their clinical applicability. Physiologically based pharmacokinetic (PBPK) modeling provides a robust framework for addressing this challenge. By mechanistically describing absorption, distribution, metabolism, and excretion (ADME) on the basis of drug-specific properties and physiological parameters, PBPK models can integrate patient-specific data to predict individual drug exposure [10].

Several PBPK models of rapamycin have previously been developed [11–13]. Early adult models characterized CYP3A-mediated metabolism and successfully predicted bioavailability, tissue distribution, and drug–drug interactions [11]. Subsequent paediatric extensions incorporated enzyme maturation and accurately described clearance in newborns and infants [12], while other work explored the pharmacogenetic effects of the CYP3A5*3 polymorphism [13]. Together, these models have advanced the quantitative understanding of sirolimus pharmacokinetics across populations and genetic profiles.

In addition to predictive performance, transparency and reproducibility are critical requirements for PBPK models intended to support cumulative model development and translational applications. However, many published PBPK models are difficult to reproduce because executable model files, full model equations, parameter sets, simulation protocols, and curated calibration or validation datasets are often not made openly available [14,15]. This limits independent verification, comparison between models, reuse in new contexts, and systematic extension by the wider community. To address these limitations, reproducible and standards-based model development is increasingly important. Encoding models in open formats such as SBML, together with openly available simulation workflows and curated pharmacokinetic datasets, provides a transparent foundation for independent evaluation, reuse, and further development in accordance with FAIR principles [16,17].

In this study, we developed a whole-body PBPK digital twin of rapamycin to simulate its pharmacokinetic profile across clinically relevant sources of variability, including food intake, CYP3A4/5 genetic polymorphisms, hepatic and renal impairment, and drug–drug interactions (DDIs). The model was developed from curated clinical pharmacokinetic data and encoded in SBML to support reproducible simulation and reuse. Together with openly available model files, simulation scripts, and curated datasets, this work provides a transparent mechanistic framework for predicting rapamycin exposure across dosing regimens and patient populations.

2. Materials and Methods

2.1. Systematic Literature Research and Data Curation

A systematic literature review was conducted to identify clinical pharmacokinetic studies of rapamycin using PubMed and PKPDAI (Figure 1). The search terms were *rapamycin AND pharmacokinetics* and *sirolimus AND pharmacokinetics*. Studies were considered eligible if they reported pharmacokinetic data in adult humans, including blood concentration–time profiles, administered dose levels, and relevant elimination parameters. Animal studies, computational modeling studies, and studies lacking the required pharmacokinetic or dosing information were excluded.

 doi:10.20944/preprints202605.0328.v1

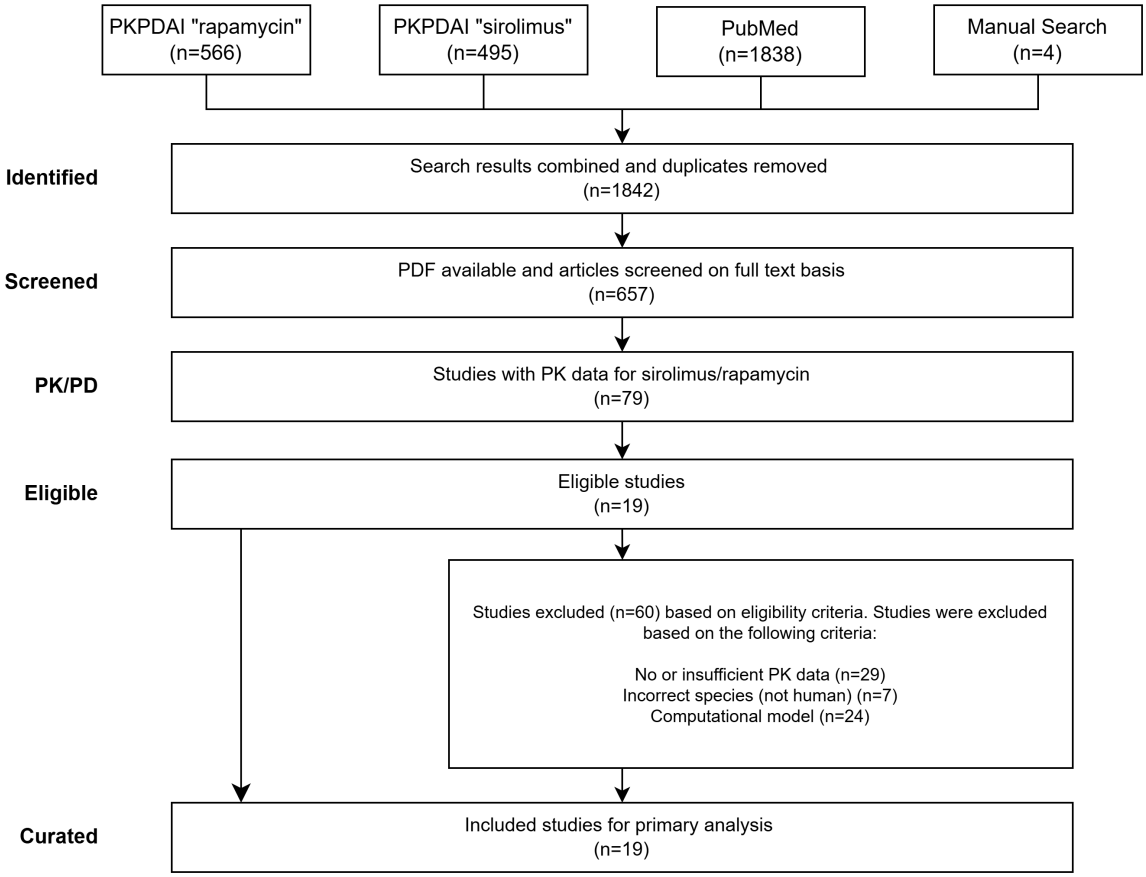

Figure 1. PRISMA workflow diagram of the literature search and study selection process.

Data from 19 eligible studies were extracted and curated in PK-DB [18]. Curated information included demographic characteristics (age, sex, and body weight), clinical status (healthy volunteers, renal or hepatic impairment, and transplant status), rapamycin dose and dosing regimen, concomitant medication, genotype information, and prandial state. Concentration–time profiles reported in figures were digitized using WebPlotDigitizer [19], and all numerical data were standardized according to the PK-DB data schema [18]. Extracted pharmacokinetic parameters included the maximum blood concentration (C_{max}), time to maximum blood concentration (t_{max}), elimination half-life ($t_{1/2}$), and area under the blood concentration–time curve (AUC).

2.2. Computational Model

A whole-body rapamycin PBPK model was developed in SBML format using sbmlutils [20]. Simulations were performed using sbmlsim [21] and libRoadRunner [22,23], visualization of the results was performed using cy3sbml [24]. The created model structure consists of absorption (oral input), distribution in organ compartments, hepatic and intestinal metabolism, and hepatic and renal excretion.

Fractional organ volumes and blood flows were taken from the literature [25]. Fractional compartment volumes were set to $FV_{gu} = 1.71\,\%$ for the gut, $FV_{ki} = 0.44\,\%$ for the kidneys, $FV_{li} = 2.10\,\%$ for the liver, and $FV_{lu} = 0.76\,\%$ for the lungs. Fractional blood flows were defined as $FQ_{gu} = 18.00\,\%$ for the gut, $FQ_{ki} = 19.00\,\%$ for the kidneys, $FQ_{h} = 21.50\,\%$ for hepatic venous outflow, and $FQ_{lu} = 100\,\%$ for the lungs. Absolute organ volumes and blood flows were calculated by scaling the corresponding fractional values by body weight.

- **Renal impairment** was modelled as a progressive reduction in renal function. The dimensionless factor f_{renal} was used to scale the renal clearance of the corresponding substances. Scaling values were derived from the KDIGO Clinical Practice Guideline for the Evaluation

 doi:10.20944/preprints202605.0328.v1

and Management of Chronic Kidney Disease [26,27]. The values were based on the estimated glomerular filtration rate (eGFR, $\mathrm{mL\,min^{-1}/1.73\,m^2}$) defining each kidney-function category: normal kidney function (eGFR $\geq$ $90\,\mathrm{mL\,min^{-1}/1.73\,m^2}$, $f_{\mathrm{renal}} = 1.00$); mild impairment ($60\,\mathrm{mL\,min^{-1}/1.73\,m^2} \leq$ eGFR $< 90\,\mathrm{mL\,min^{-1}/1.73\,m^2}$, $f_{\mathrm{renal}} = 0.69$); moderate impairment ($30\,\mathrm{mL\,min^{-1}/1.73\,m^2} \leq$ eGFR $< 60\,\mathrm{mL\,min^{-1}/1.73\,m^2}$, $f_{\mathrm{renal}} = 0.32$); severe impairment ($15\,\mathrm{mL\,min^{-1}/1.73\,m^2} \leq$ eGFR $< 30\,\mathrm{mL\,min^{-1}/1.73\,m^2}$, $f_{\mathrm{renal}} = 0.24$); and end-stage kidney disease (eGFR $< 15\,\mathrm{mL\,min^{-1}/1.73\,m^2}$, $f_{\mathrm{renal}} = 0.10$). Dialysis was not included in the model.

- **Hepatic impairment** was modelled as a progressive reduction in functional liver tissue and an increase in portosystemic shunting. The dimensionless factor $f_{\mathrm{cirrhosis}}$ represents the fraction of non-functional liver parenchyma and the development of portosystemic collaterals. Values were assigned according to Child–Turcotte–Pugh (CTP) classes, which are used to classify the severity of cirrhosis and estimate prognosis: class A (mild impairment, 5–6 points, $f_{\mathrm{cirrhosis}} = 0.40$); class B (moderate impairment, 7–9 points, $f_{\mathrm{cirrhosis}} = 0.70$); and class C (severe impairment, 10–15 points, $f_{\mathrm{cirrhosis}} = 0.81$) [28–31].

2.3. Model Parametrization

The parameters of the model were estimated by minimizing the weighted sum of squared residuals between model simulations and available clinical observations. The objective function was defined as

$$F(\vec{p}) = \frac{1}{2}\sum_{i,k}(w_{i,k} \cdot r_{i,k}(\vec{p}))^2,$$

where $r_{i,k}(\vec{p})$ is the residual between the observed concentration and the corresponding model prediction for observation i in study k, and $w_{i,k}$ represents the weighting factor accounting for study sample size and measurement variance. Model calibration was performed simultaneously across fed and fasted conditions and across the available dose levels to capture variability between physiological states and dosing regimens.

To reduce the likelihood of convergence to local optima and improve the robustness of the parameter estimates, 100 independent optimization runs were performed from distinct starting points. Model performance was subsequently assessed using goodness-of-fit plots.

2.4. Pharmacokinetic Parameters

The pharmacokinetic parameters (C_{max}, t_{max}, AUC, $t_{1/2}$, and CL/F) were derived from the concentration–time profiles reported in the selected clinical studies using non-compartmental analysis. AUC values were calculated by trapezoidal integration, with extrapolation of the terminal phase where applicable. The simulated concentration–time profiles and corresponding pharmacokinetic parameters were then compared with the curated experimental data to assess the model's ability to reproduce observed pharmacokinetic behaviour.

3. Results

3.1. Rapamycin Database

Clinical pharmacokinetic data for rapamycin were curated from 19 independent studies and assembled into an open-access database (Table 1). Following the systematic literature review (Figure 1), the included studies covered a broad range of dosing regimens, physiological states, and genotype variants (Table 1). This integrated dataset provided the foundation for model development, parametrization, and evaluation.

 doi:10.20944/preprints202605.0328.v1

Table 1. Summary of studies for modeling. Overview of study identifiers, PK-DB IDs, PMID, route, dosing, and subject characteristics, including health status (H), hepatic impairment (HI), renal impairment (RI), and renal transplant (RT).

Study	PK-DB	PMID	Route	Dosing	Dose	Dose unit	DDI	Genotype	H	Fed	HI	RI	RT
[2]	PKDB01078	31089971	PO	single	0.5, 2, 10, 40	mg			✓	✓			
[42]	PKDB01038	11180036	PO	single	10	mg	Diltiazem		✓				
[33]	PKDB01003	11034258	PO	single	0.3, 1, 3, 5, 8	[mg/m^2]			✓				
[36]	PKDB01079	10594869	PO	multi	3.6 ± 1.1	mg	Cyclosporine						✓
[5]	PKDB01004	27121219	PO	single	5	mg			✓				
[35]	PKDB01006	16623021	PO	single	6	mg			✓				
[8]	PKDB01073	16418694	PO	single	40	mg			✓				
[39]	PKDB01080	17192769	PO	single	2.9 ± 2.26	mg		CYP3A5 1*/1*, *1/*3, *3/*3					✓
[37]	PKDB01081	18482049	PO	single	6	mg	Tacrolimus, Mycophenolate motefil				✓		
[44]	PKDB01005	23052408	PO	single	15	mg	Tacrolimus		✓				
[43]	PKDB01007	27128230	PO	single	20	mg	Rifampin		✓				
[46]	PKDB01082	27128614	PO	multiple	1-4	mg	Cyclosporine	CYP3A5 1*/1*, *1/*3, *3/*3					✓
[41]	PKDB01070	36416673	PO	single	2	mg	Ritonavir, Ombitasivir, Paritaprevir, Dasabuvir		✓				
[40]	PKDB01071	28700521	PO	single	5	mg		CYP3A4 1*/1*, *1/*1G, *1G/*1G; CYP3A5 1*/1*, *1/*3, *3/*3	✓				
[34]	PKDB01083	9156373	PO	multiple	0.5, 1, 1.5, 2.5, 3, 3.5, 4, 5, 6.5	mg/m^2	Cyclosporine						✓
[48]	PKDB01084	10579146	PO	single	15	mg			✓	✓			
[45]	PKDB01072	18218785	PO	single	15	mg	Cyclosporine		✓				
[47]	PKDB01085	16291711	PO	single	15	mg					✓		
[38]	PKDB01086	18218785	PO	single	15	mg					✓		

 doi:10.20944/preprints202605.0328.v1

3.2. Computational Model

A whole-body PBPK model of rapamycin was developed to represent the major physiological and drug-specific processes governing its pharmacokinetics (Figure 2). The model describes the anatomical compartments relevant to rapamycin absorption, distribution, metabolism, and excretion, including the gastrointestinal tract, liver, kidneys, and systemic circulation. Drug-specific processes included dissolution and intestinal absorption, CYP-mediated intestinal and hepatic metabolism, faecal elimination, and renal excretion.

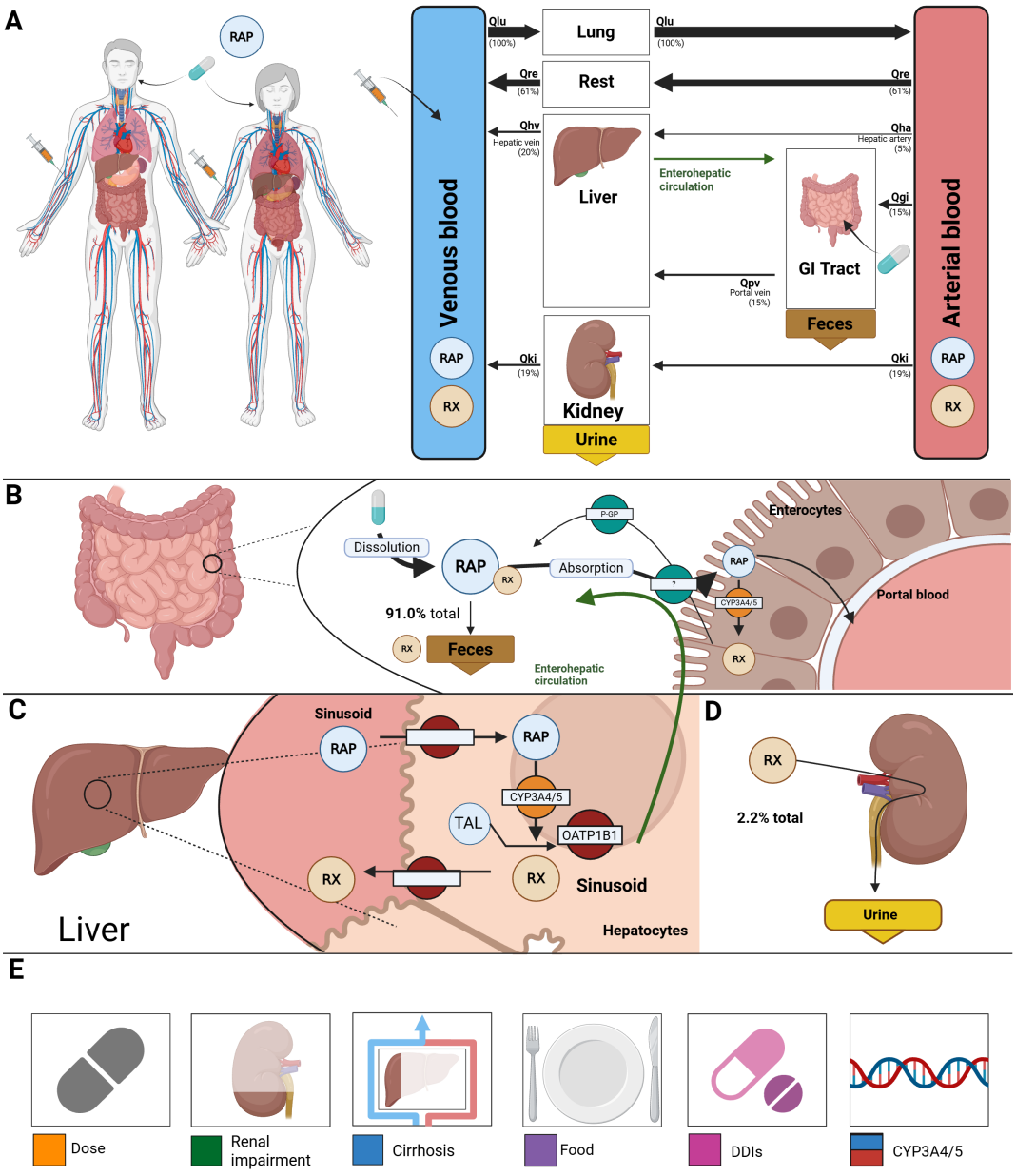

Figure 2. Whole-body PBPK model of rapamycin and key factors influencing its disposition. A) Whole-body model of rapamycin (RAP) administration (oral and intravenous), its systemic circulation via blood circulatory system, and key organs involved in its metabolism, distribution, and excretion. **B)** Intestine model illustrating rapamycin absorption by enterocytes. **C)** Hepatic model of RAP uptake by hepatocytes and its conversion to metabolites by CYP3A4 and CYP3A5. **D)** Renal model describing excretion of rapamycin in urine via kidneys. **E)** Key factors affecting rapamycin disposition accounted for in the model: dose, renal function, cirrhosis, food effect, CYP3A4 and CYP3A5 activity.

Key sources of intra- and inter-individual variability were explicitly incorporated into the model structure. These included dose level, nutritional state (fasted or fed), CYP3A4/5 genotype, and

 doi:10.20944/preprints202605.0328.v1

the presence of renal or hepatic impairment. Together, these components enabled the simulation of clinically relevant variability in rapamycin exposure across different physiological states and patient populations.

The complete model, including simulation scripts and documentation, is available in SBML format under a CC-BY 4.0 license via GitHub (https://github.com/matthiaskoenig/rapamycin-model) and is archived on Zenodo (v0.5.0) [32].

3.3. Dose Dependency

The dose dependency of rapamycin pharmacokinetics was evaluated for oral doses ranging from 0.5 mg to 40 mg and from 0.3 mg m^{-2} to 8 mg m^{-2}. Across studies in healthy volunteers and stable renal transplant recipients, rapamycin was rapidly absorbed, with peak blood concentrations typically reached within 1 h to 2 h. Pronounced inter-individual variability was observed across the reported concentration–time profiles. Rapamycin was extensively distributed into formed blood elements, consistent with the substantially higher concentrations reported in whole blood compared with plasma.

Dose-dependency simulations reproduced the observed increase in systemic exposure with increasing dose. Exposure metrics, including C_{max} and AUC, increased approximately proportionally with dose, whereas elimination-related parameters, including the elimination rate constant k_{el} and terminal half-life $t_{1/2}$, remained largely independent of the administered dose. These findings are consistent with dose-linear pharmacokinetics over the investigated dose range.

Time-course simulations were performed for all curated clinical dose and dose-dependency studies (Basa-Denes2019 [2], Brattstrom2000 [33], Zimmerman1997 [34], Leelahavanichkul2005 [35], KorthBradley2012 [5], Kelly1999 [36], Leung2006 [8]). Simulated rapamycin concentrations in blood and plasma, as well as urinary and faecal excretion, are shown for single- and multiple-dose regimens. Direct comparison was possible for blood concentration–time profiles, whereas plasma concentrations, metabolite profiles, and urinary and faecal excretion data were not available in the curated clinical studies.

3.4. Renal Impairment

The pharmacokinetics of rapamycin under conditions of renal impairment appeared to be relatively stable. Across the evaluated degrees of renal impairment, simulated rapamycin exposure showed only minor changes, indicating that systemic exposure is largely insensitive to reduced renal function. This finding is consistent with the predominant elimination pathway of rapamycin, which is mainly governed by hepatic metabolism and biliary/faecal excretion rather than renal clearance.

However, interpretation of these results is limited by the fact that the available clinical data for model evaluation were derived from a single study in patients who had undergone Roux-en-Y gastric bypass surgery. In this population, observed rapamycin exposure was lower than predicted, and substantial inter-individual variability was reported for both peak concentrations and overall exposure. These discrepancies are therefore more likely attributable to altered gastrointestinal anatomy and impaired absorption after gastric bypass than to renal impairment itself.

Roux-en-Y gastric bypass reduces the absorptive surface area of the proximal intestine and alters gastrointestinal physiology, including gastric pH, intestinal transit, and drug dissolution conditions. For rapamycin, which has limited aqueous solubility and absorption that depends on gastrointestinal conditions, these changes may substantially reduce oral bioavailability [37]. Because the model does not currently account for malabsorptive changes following bariatric surgery, the agreement between simulations and clinical observations was weaker in this scenario than in other evaluated populations.

Taken together, the simulations suggest that renal impairment alone has only a minor effect on rapamycin pharmacokinetics. In contrast, gastrointestinal factors affecting absorption may represent a more important source of variability in specific patient populations. Additional clinical pharmacokinetic data from patients with renal impairment but without concomitant bariatric surgery would

 doi:10.20944/preprints202605.0328.v1

be required to more clearly distinguish the effects of renal dysfunction from those of altered oral absorption.

3.5. Hepatic Impairment

The effect of hepatic impairment on rapamycin pharmacokinetics was evaluated using simulations based on data from patients with severe liver cirrhosis (Child–Pugh class C; Figure 5). Simulations were performed across hepatic function states ranging from normal liver function to severe cirrhosis. Rapamycin exposure increased with declining liver function, as reflected by higher AUC and a prolonged terminal half-life. This was accompanied by a progressive decrease in the elimination rate constant k_{el}, consistent with reduced hepatic clearance under impaired liver function. In contrast, C_{max} remained largely unchanged across the simulated degrees of cirrhosis, indicating that hepatic impairment primarily affected elimination rather than the initial absorption phase.

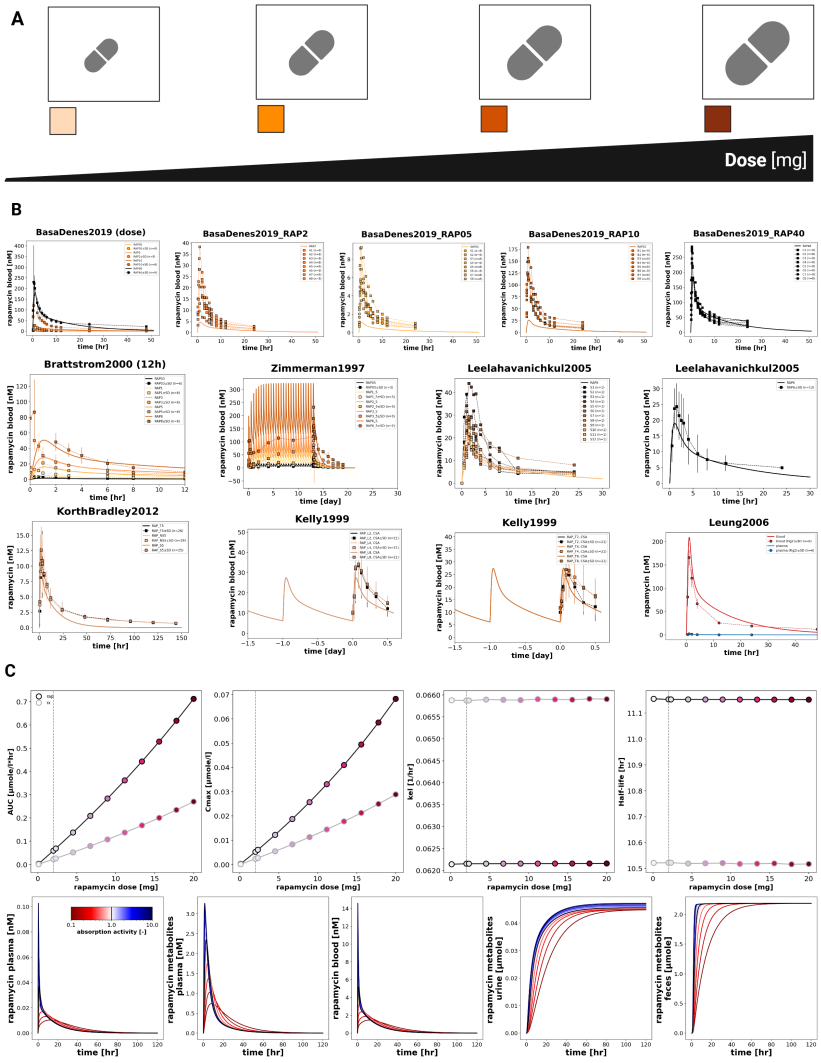

Figure 3. Dose-dependent pharmacokinetics of rapamycin. A) Oral dose range (0–40 mg). **B)** Pharmacokinetic time courses of rapamycin in the blood and plasma. **C)** Pharmacokinetic parameters (AUC_{0-inf}, C_{max}, k_{el}, and half-life) for rapamycin; observed parameters overlaid where available. **D)** Comparison of simulations with study data from BasaDenes2019 [2], Brattstrom2000 [33], Zimmerman1997 [34], Leelahavanichkul2005 [35], KorthBradley2012 [5], Kelly1999 [36], Leung2006 [8]. Simulations are shown as solid lines and study data as symbols with SDs where available.

 doi:10.20944/preprints202605.0328.v1

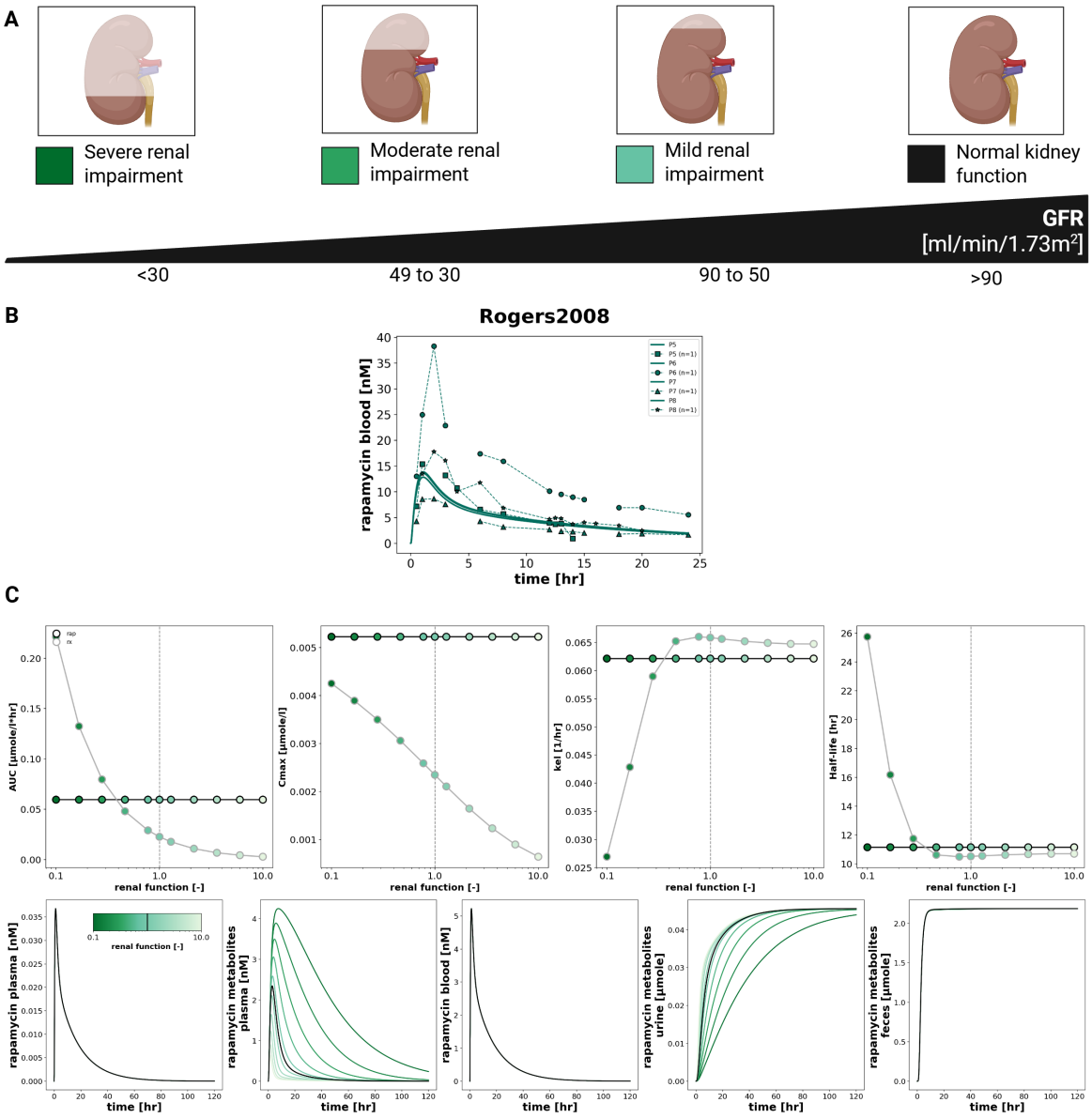

Figure 4. Effect of renal impairment on pharmacokinetics of rapamycin. A) Renal function categories from normal to severe impairment used in simulations. **B)** Pharmacokinetic time courses of rapamycin in the blood. **C)** Pharmacokinetic parameters ($AUC_{0-\inf}$, $C_{\max}$, k_{el}, and half-life) for rapamycin; observed parameters overlaid where available. **D)** Comparison of simulations with study data Rogers2008 [37]. Simulations are shown as solid lines, and study data as symbols with SDs where available.

For rapamycin metabolites, increasing hepatic impairment resulted in reduced metabolite formation in plasma and a corresponding decrease in cumulative metabolite excretion. These findings are consistent with the reduced CYP-mediated metabolic capacity and altered hepatic blood flow associated with cirrhosis.

Simulated blood concentration–time profiles of the parent compound and metabolites, together with urinary and faecal excretion profiles, are shown for the different hepatic function groups and compared with the available clinical data from Zimmerman2008 [38]. Direct comparison was possible for whole-blood rapamycin concentration–time profiles, whereas plasma concentrations, metabolite profiles, and urinary and faecal excretion data were not available in the curated clinical study.

Preprints.org (www.preprints.org) | NOT PEER-REVIEWED | Posted: 6 May 2026 doi:10.20944/preprints202605.0328.v1

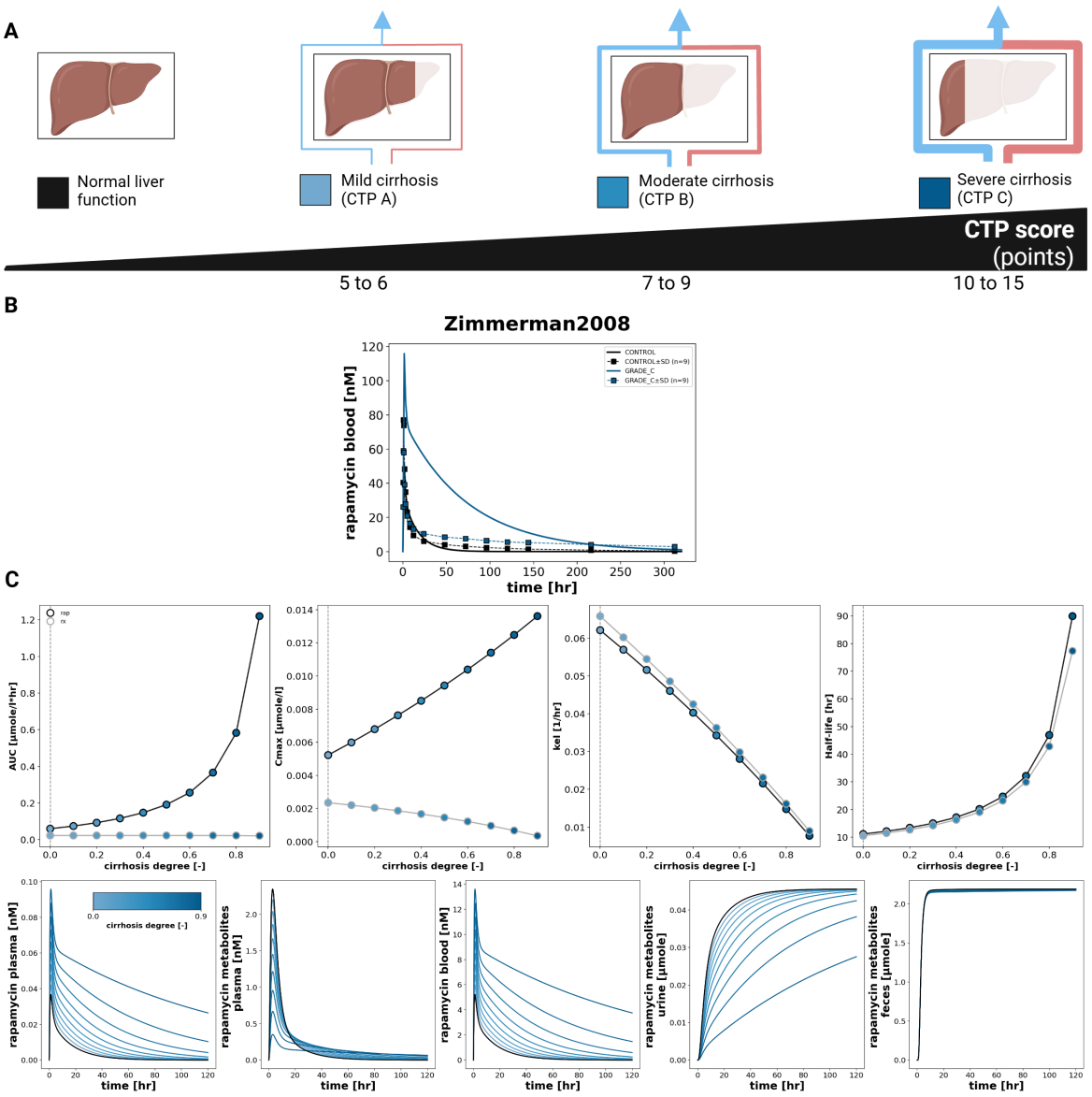

Figure 5. Effect of hepatic impairment on pharmacokinetics of rapamycin. A) Liver function categories used in simulations. **B)** Pharmacokinetic time courses of rapamycin in the blood. **C)** Pharmacokinetic parameters (AUC_{0-inf}, C_{max}, k_{el}, and half-life) for rapamycin; observed parameters overlaid where available. **D)** Comparison of simulations with study data Zimmerman2005 [47], Zimmerman2008 [38]. Simulations are shown as solid lines, and study data as symbols with SDs where available.

3.6. Food Effect

The effect of food on rapamycin pharmacokinetics was evaluated using simulations under fed and fasted conditions (Figure 6). Following oral administration with food, the initial absorption phase was altered, resulting in a lower maximum whole-blood concentration C_{max} and a delayed time to peak concentration. Compared with the fasted state, the fed state produced a lower and broader concentration–time profile, whereas the fasted state was characterized by more rapid absorption and a sharper peak.

Total systemic exposure was largely preserved, indicating that food primarily affected the rate of absorption rather than the overall extent of absorption. Consistently, simulated plasma metabolite profiles were flattened under fed conditions, whereas the cumulative amount of excreted metabolites remained largely unchanged.

 doi:10.20944/preprints202605.0328.v1

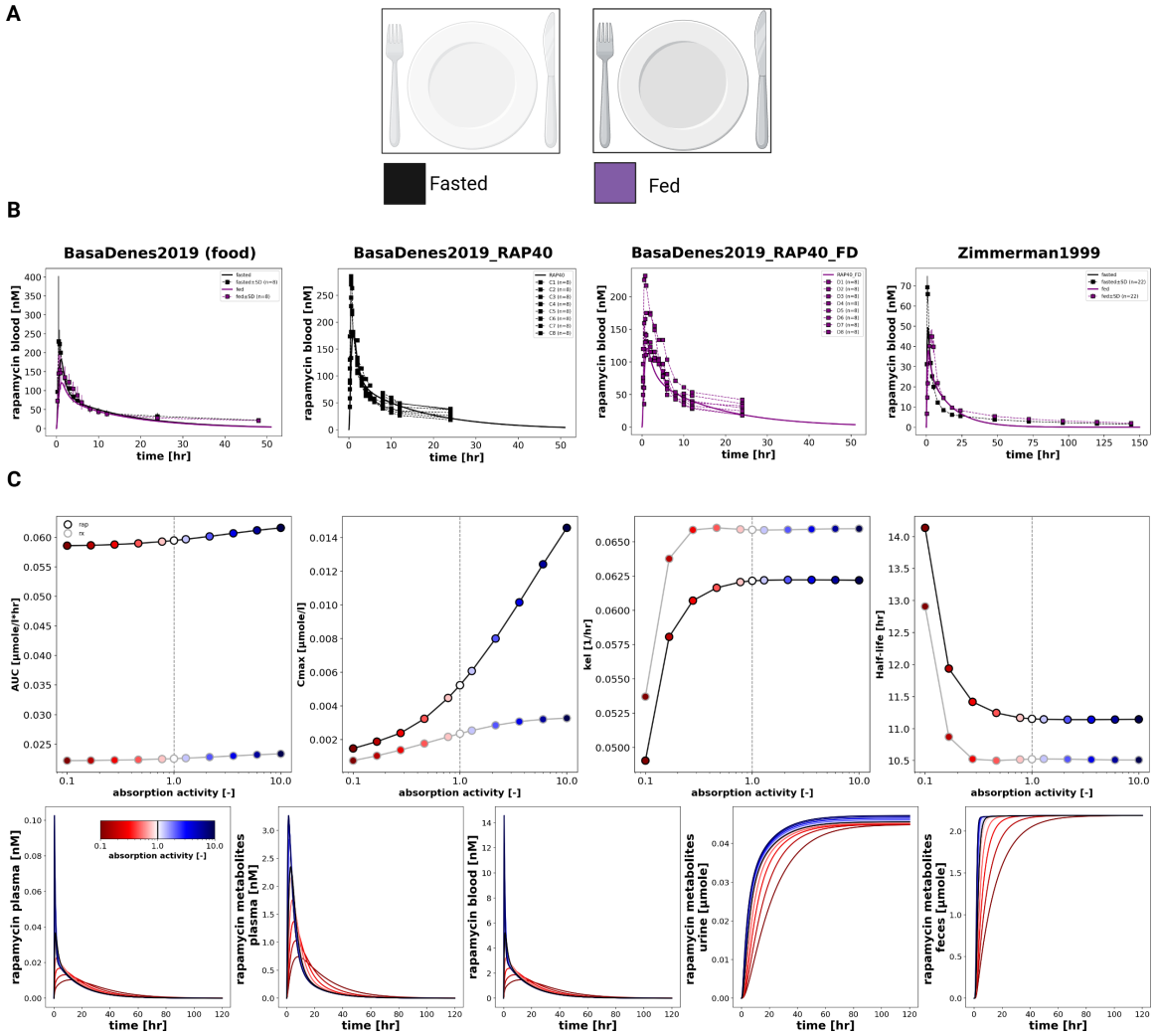

Figure 6. Effect of gestational state on pharmacokinetics of rapamycin. A) Gestational state categories used in simulations. **B)** Pharmacokinetic time courses of rapamycin in the blood. **C)** Pharmacokinetic parameters (AUC_{0-inf}, C_{max}, k_{el}, and half-life) for rapamycin; observed parameters overlaid where available. **D)** Comparison of simulations with study data Basa-Denes2019 [2], Zimmerman1999 [48]. Simulations are shown as solid lines, and study data as symbols with SDs where available.

Simulated blood concentration–time profiles of the parent compound and metabolites, together with urinary and faecal excretion profiles, are shown for fed and fasted conditions and compared with the available clinical data from Zimmerman2008 [38] and Basa-Denes2019 [2]. Direct comparison was possible for whole-blood rapamycin concentration–time profiles, whereas plasma concentrations, metabolite profiles, and urinary and faecal excretion data were not available in the curated clinical studies.

3.7. Genetic Variants (CYP3A4 and CYP3A5)

The effects of CYP3A4 and CYP3A5 genetic variants on rapamycin pharmacokinetics are shown in Figure 7. Genetic polymorphisms affected inter-individual variability in rapamycin exposure through changes in organ-specific metabolic activity. Clinical concentration–time profiles indicated that the CYP3A4*1G variant and CYP3A5*1 expressor status were associated with increased metabolic activity and lower whole-blood rapamycin concentrations compared with the corresponding lower-activity or non-expressor genotypes.

 doi:10.20944/preprints202605.0328.v1

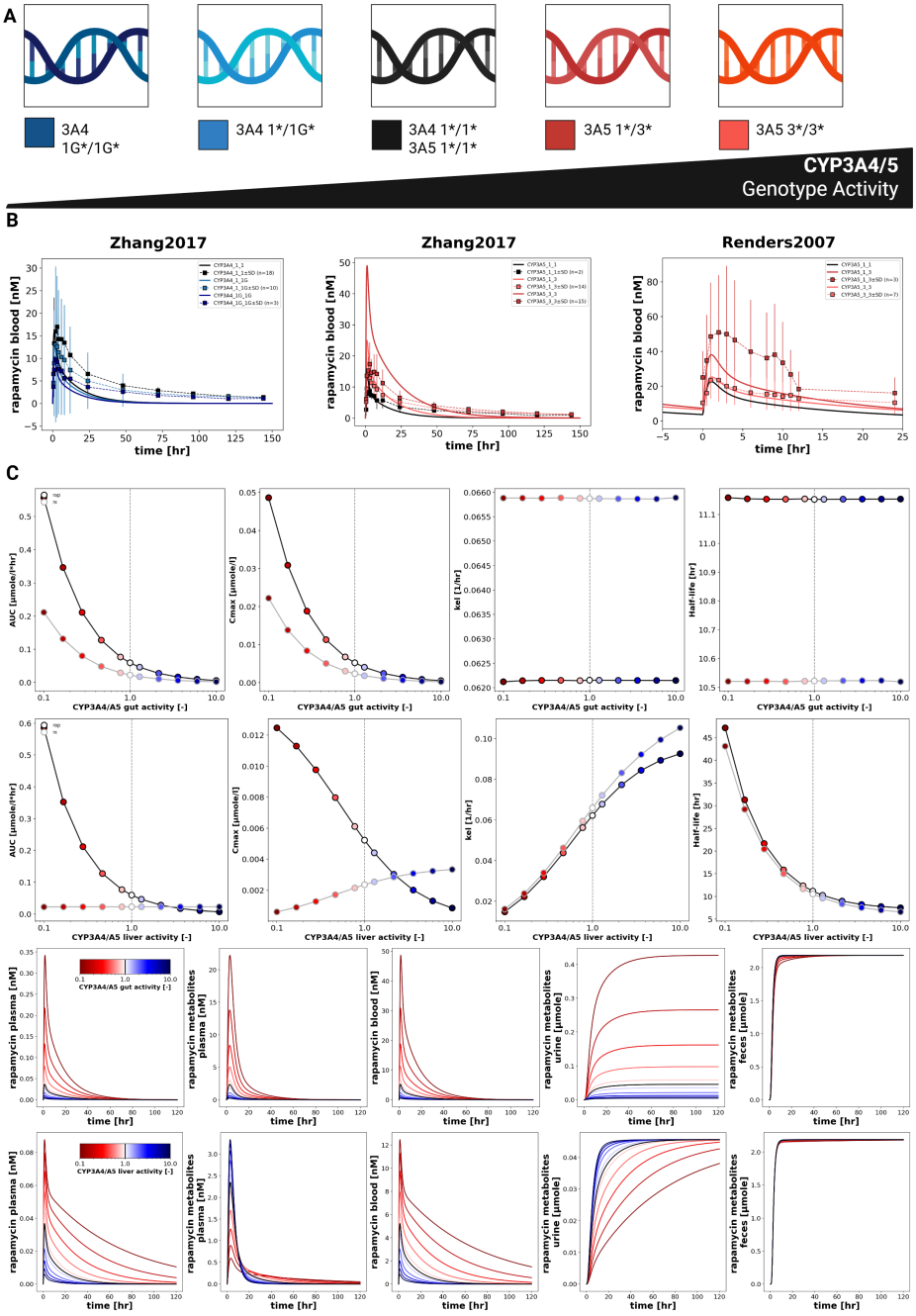

Figure 7. Effect of CYP3A4/5 genotype on pharmacokinetics of rapamycin. A) CYP3A4/5 genotype activity categories used in simulations. **B)** Pharmacokinetic time courses of rapamycin in the blood. **C)** Pharmacokinetic parameters ($AUC_{0-\text{inf}}$, C_{max}, k_{el}, and half-life) for rapamycin in the gut and liver; observed parameters overlaid where available. **D)** Comparison of simulations with study data Zhang2017 [40], Renders2007 [39]. Simulations are shown as solid lines, and study data as symbols with SDs where available.

For both CYP3A4 and CYP3A5, increased hepatic enzyme activity resulted in reduced rapamycin exposure, reflected by lower AUC and shorter terminal half-life. This was accompanied by an increase in the elimination rate constant k_{el}, consistent with enhanced systemic clearance. In contrast, increased intestinal enzyme activity primarily reduced bioavailability, leading to lower AUC and C_{max}, while k_{el} and terminal half-life remained largely unchanged. These findings indicate that intestinal CYP activity mainly affects first-pass metabolism and absorption-related exposure, whereas hepatic CYP activity determines systemic elimination after absorption.

 doi:10.20944/preprints202605.0328.v1

Across both enzymes, higher-activity genotypes shifted the metabolic profile towards increased metabolite formation, resulting in higher simulated plasma metabolite concentrations and increased cumulative urinary excretion of metabolites, while faecal excretion remained largely unchanged.

Simulated blood concentration–time profiles of the parent compound and metabolites, together with urinary and faecal excretion profiles, are shown for the CYP3A4 and CYP3A5 genotype groups and compared with the available clinical data from Renders2007 [39] and Zhang2017 [40]. Direct comparison was possible for whole-blood rapamycin concentration–time profiles, whereas plasma concentrations, metabolite profiles, and urinary and faecal excretion data were not available in the curated clinical studies.

3.8. Drug-Drug Interactions (DDIs)

Rapamycin pharmacokinetics was strongly influenced by co-administered drugs targeting CYP3A4 and P-glycoprotein pathways (Figure 8). In healthy volunteers, CYP3A4 inhibition increased rapamycin exposure. The 3D regimen containing ritonavir increased whole-blood rapamycin concentrations and prolonged the terminal half-life [41]. Diltiazem similarly increased rapamycin exposure, consistent with reduced intestinal and hepatic CYP3A4-mediated first-pass metabolism [42]. By contrast, rifampin markedly decreased rapamycin exposure, consistent with CYP3A4 and P-glycoprotein induction and enhanced clearance [43]. Tacrolimus had only a minor effect on rapamycin pharmacokinetics in healthy subjects, with simulated concentration–time profiles closely matching those obtained after rapamycin administration alone [44].

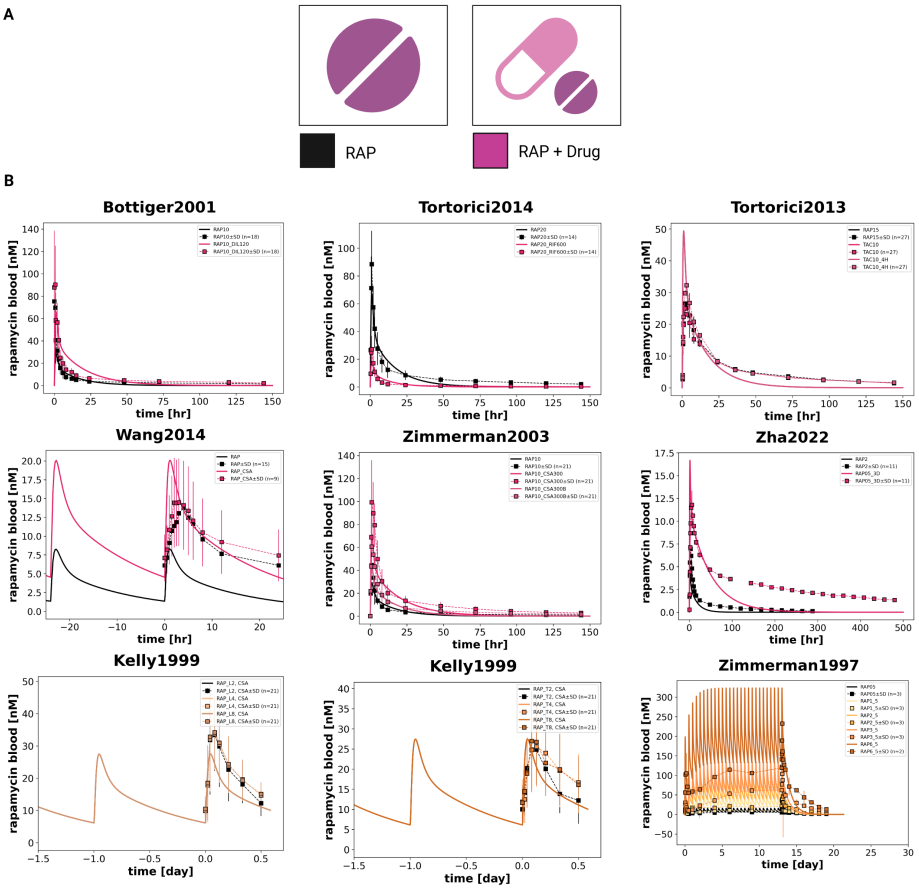

Figure 8. Effect of co-administered drugs on pharmacokinetics of rapamycin. A) Drug administration categories used in simulations. **B)** Pharmacokinetic time courses of rapamycin in the blood. **C)** Comparison of simulations with study data Bottiger2001 [42], Tortorici2013 [44], Tortorici2014 [43], Wang2014 [46], Zimmerman2003 [45], Zha2022 [41], Kelly1999 [36], Zimmerman1997 [34]. Simulations are shown as solid lines, and study data as symbols with SDs where available.

 doi:10.20944/preprints202605.0328.v1

In stable renal transplant recipients, simulated rapamycin concentrations remained stable during maintenance therapy with cyclosporine when staggered dosing was considered. Although cyclosporine co-administration markedly increases rapamycin exposure in healthy subjects [45], this interaction can be reduced by separating the dosing times. The simulations therefore reproduced stable and predictable rapamycin concentration–time profiles under clinically used maintenance regimens in transplant patients [34,36,46].

4. Discussion

4.1. Model

This work established a curated clinical dataset of rapamycin pharmacokinetics and used it to develop a whole-body mechanistic PBPK model. In total, 19 previously published clinical studies were curated, covering a broad range of rapamycin dosing regimens and patient populations. This enabled the evaluation of clinically relevant factors affecting rapamycin exposure, including dose level, food intake, renal and hepatic impairment, genetic variability, and drug–drug interactions.

Although data availability was limited, the curated dataset was sufficient for model development and evaluation. Whole-blood concentration–time profiles were consistently reported across studies, including single-dose, multiple-dose, staggered-dose, and maintenance-therapy regimens. In contrast, plasma concentration profiles, metabolite data, and urinary or faecal excretion data were generally unavailable, limiting direct validation of these model components.

The developed framework integrates systemic circulation, hepatic and intestinal metabolism, and renal elimination into a mechanistic whole-body representation of rapamycin pharmacokinetics. Parameter optimization and the agreement between simulated and observed concentration–time profiles across the evaluated studies support the reliability of the model, while also providing a basis for future refinement as additional clinical pharmacokinetic data become available. A key advantage of this mechanistic modelling approach is its ability to investigate clinically relevant scenarios that are difficult to assess systematically in clinical trials, such as organ impairment, genetic variability, drug–drug interactions, or changes in dosing regimens under controlled *in silico* conditions.

4.2. Dose Dependency

Simulations of rapamycin dose dependency showed good agreement with published clinical data and captured the major pharmacokinetic trends across a broad range of dosing regimens. The model reproduced the approximately dose-proportional increase in peak whole-blood concentrations C_{max} and total exposure AUC observed across the curated studies. It also captured the characteristic long terminal half-life of rapamycin. In multiple-dose scenarios, the model reproduced the accumulation phase, consistent with clinical observations that sirolimus concentrations increase over several days before reaching steady state. Although simulated profiles did not perfectly overlap with all observed data, this is expected given the pronounced inter-individual variability reported for rapamycin pharmacokinetics.

4.3. Renal Impairment

Pharmacokinetics of rapamycin under conditions of renal impairment appear to be relatively stable. However, the evaluation of this effect was limited as it was based on a single simulated study in which patients had undergone gastric bypass surgery. This study reported substantial inter-patient variability in peak concentrations and overall exposure, which contributed to discrepancies between simulated and observed data.

Across the assessed levels of renal impairment, simulated rapamycin exposure showed only minimal changes, suggesting that systemic exposure is largely insensitive to declining renal function. This observation is consistent with the known elimination pathway of rapamycin, which primarily involves hepatic metabolism and faecal excretion rather than renal clearance.

 doi:10.20944/preprints202605.0328.v1

Despite these simulation trends, the clinical data used for model validation demonstrated lower exposure than predicted. This discrepancy is most likely attributable to the effects of Roux-en-Y gastric bypass in the study population rather than renal impairment itself. The surgical procedure reduces the absorptive surface area of the proximal intestine and alters gastric pH, thereby decreasing rapamycin solubility and absorption [37].

The agreement between simulations and clinical observations in the context of renal impairment was weaker than in other populations, likely because the mechanistic model does not account for malabsorptive changes following bypass. These findings suggest that while rapamycin pharmacokinetics are not inherently sensitive to renal function, other physiological factors may play a more significant role in driving inter-individual variability.

4.4. Hepatic Impairment

In contrast, the pharmacokinetics of rapamycin under conditions of hepatic impairment show a clear dependence on liver function, although available data remain limited. Evaluation in this population is based on a single reported blood concentration-time profile, which exhibits substantial inter-individual variability and complicates direct quantitative comparisons between simulation and observed data.

Clinical findings indicate a progressive and significant increase in systemic exposure, along with a prolongation of the terminal half-life, as the severity of liver dysfunction increases. Rapamycin exposure rises with advancing cirrhosis, reflecting a consistent reduction in systemic clearance. In subjects with severe hepatic impairment (Child-Pugh C), these pharmacokinetic parameters are markedly altered compared with healthy individuals. Conversely, the absorption phase appears to be largely unaffected by hepatic status, while reduced clearance is the dominant and consistently observed change.

Model simulations accurately predict these trends, reflecting the diminished hepatic metabolic capacity. Despite the general agreement between simulations and clinical trends, the high variability observed among patients suggests that additional processes can contribute to the disposition of rapamycin, such as the effects of liver cirrhosis on the activity of CYP3A4 and CYP3A5 that reduce the metabolic capacity of the subject, the abundance of intestinal CYP3A4 protein, or the activity of the P-glycoprotein efflux pump in the small intestine.

Model simulations capture these trends adequately, reflecting diminished hepatic metabolic capacity. However, despite general agreement between simulated and observed data, the pronounced variability among patients suggests that additional factors may influence rapamycin disposition. These may include alterations in the activity of CYP3A4 and CYP3A5 enzymes, reduced intestinal CYP3A4 abundance, and changes in the activity of the P-glycoprotein efflux transporters in the small intestine.

4.5. Food Effect

The effect of prandial state on rapamycin pharmacokinetics is moderate but becomes more pronounced following high-fat meals. Clinical data indicate that food primarily alters the rate of absorption, while its impact on total systemic exposure depends on the formulation. For the oral solution, administration with high-fat meal results in a reduction in maximum blood concentration (C_{max}) and a marked delay in time to peak concentration (t_{max}), with only a moderate increase in overall exposure. In contrast, tablet formulations have been associated with increases in both C_{max} and AUC under fed conditions, whereas nano-amorphous formulations show reduced peak concentrations without significant changes in total exposure. Despite these formulation-dependent differences in absorption, the terminal half-life remains unaffected by food intake.

Model simulations reproduce these trends well, including the delayed and attenuated peak concentrations observed in the fed state. The impact of food is primarily reflected in altered absorption kinetics, leading to variability in peak concentrations and apparent elimination profiles, while overall exposure remains relatively stable. By incorporating mechanistic descriptions of gastrointestinal processes, the model captures the effects of delayed gastric emptying and enhanced solubilization

 doi:10.20944/preprints202605.0328.v1

mediated by dietary fats and bile salts. Furthermore, inclusion of intestinal and liver metabolic pathways enables the model to account for potential modulation of CYP3A4 and CYP3A5 activity in the gastrointestinal tract, including competitive inhibition or transient reduction in metabolic capacity associated with food intake.

The agreement between simulations and clinical observations for the food effect is generally robust, although the differences can be caused mostly by inter-individual variability and food components interactions with P-gp, which the model does not account for. These findings suggest that while food is a relevant factor, other intrinsic processes such as enzymatic variability and genetic polymorphisms can significantly influence the effect of prandial state on the disposition of rapamycin.

Overall, the agreement between simulations and clinical observations for the food effect is satisfactory, although some discrepancies remain. There are likely attributable to inter-individual variability and food-drug interactions involving transport proteins (P-gp), which are not captured by the model. Collectively, these finding indicate that while prandial state is an important determinant of rapamycin absorption kinetics, intrinsic factors such as enzyme variability and its genetic polymorphisms may further modulate its overall pharmacokinetic profile.

4.6. Genetic Polymorphisms

Genetic variability in the metabolic enzymes CYP3A4 and CYP3A5 represents an important source of inter-individual differences in rapamycin pharmacokinetics. Sirolimus is a sensitive substrate of both enzymes, which contribute to extensive first-pass metabolism in the liver and intestinal wall. Evaluation in this context demonstrated substantial variability between individuals, particularly in parameters such as clearance and volume of distribution.

Clinical data indicate that enzyme activity is an important determinant of rapamycin disposition. Individuals carrying the functional CYP3A5*1 allele (expressors) generally exhibit higher oral clearance than those homozygous for the inactive CYP3A5*3 variant. In parallel, variability in CYP3A4 has been associated with genotypes such as *1/*1, *1/*1G, and *1G/*1G, reflecting polymorphisms that contribute to differences in metabolic capacity, with particularly notable effects reported in Asian populations.

To mechanistically account for this variability, the model incorporates both hepatic and intestinal metabolism mediated by CYP3A4 and CYP3A5, including the influence of genetic polymorphisms. Within this framework, genotype-dependent effects are represented by assigning relative enzyme activity levels corresponding to differences in metabolic capacity. Although some discrepancies between simulations and observed data remain, the model captures the overall trends associated with genetic variation. In particular, reduced enzymatic activity in either the liver or intestine leads to increased systemic exposure and prolongation of the terminal half-life.

4.7. Drug-Drug Interactions (DDIs)

Drug–drug interactions represent an important modulator of rapamycin pharmacokinetics, primarily through effects on shared metabolic enzymes and transporters. These interactions predominantly involve the CYP3A4-mediated metabolic pathway, which is incorporated into the model to account for competitive, inhibitory, and inductive effects arising from concomitant drug administration. Within this framework, inhibition or induction is represented by adjusting relative enzyme activity levels to capture general interaction trends.

Clinical data demonstrate that strong CYP3A4 inhibitors, such as diltiazem and ritonavir, significantly increase systemic exposure and prolong the terminal half-life of rapamycin. Similarly, co-administration with cyclosporine leads to a marked increase in rapamycin blood concentrations; however, this effect can be mitigated by separating the dosing times by several hours. In contrast, potent CYP3A4 inducers, such as rifampin, substantially enhance drug clearance, resulting in reduced systemic exposure. Tacrolimus, despite its structural similarity to rapamycin, does not exhibit clinically meaningful pharmacokinetic interactions.

 doi:10.20944/preprints202605.0328.v1

Model simulations reproduced these interaction patterns, capturing the main trends observed under both simultaneous and staggered dosing regimens across different therapeutic combinations. Remaining discrepancies between simulated and observed data are likely attributable to the high inter-individual variability associated with rapamycin, limited clinical data, and additional factors such as variability in enzyme expression and population-specific differences.

4.8. Outlook

Future efforts aimed at advancing models of rapamycin and other immunosuppressive agents should prioritize the standardization and enhancement of reported clinical data. Equally important is a deeper exploration of rapamycin's mechanism of action to address existing knowledge gaps. In particular, further research is needed to better characterize the effects of organ impairment on pharmacokinetics, as well as the role of genetic polymorphisms in inter-individual variability. Moreover, quantifying the specific contributions of CYP3A enzymes and P-glycoprotein transporters to sirolimus disposition and activity remains essential for improving mechanistic understanding and predictive accuracy, and ultimately for optimizing therapeutic outcomes.

The model successfully captured general trends in the ADME profile of rapamycin; however, the available data remain limited, particularly with respect to its metabolites and detailed excretion patterns in urine and faeces. As a result, these predictions could not be fully validated against clinical observations. Improved availability of such data would enable more comprehensive model refinement and validation, while also enhancing the applicability of mechanistic PBPK models for a deeper understanding of the drug's behaviour and therapeutic efficacy in patients.

4.9. Reproducibility

Beyond the pharmacological insights, this study highlights a broader challenge in computational pharmacology and systems biology related to model transparency and reproducibility. A considerable proportion of published PBPK models cannot be independently reproduced, because critical components such as model equations, executable code, and well-curated calibration datasets are often not made publicly accessible. This lack of availability limits independent validation and substantially constrains the reuse, extension, and cumulative advancement of models within the scientific community.

To address these limitations, reproducibility and accessibility of the whole-body rapamycin PBPK model were established as central design principles of the present work. The complete modelling framework, including the SBML-encoded model, simulation scripts, and curated clinical datasets, is made openly available and organized according to the FAIR principles [16,17]. This ensures that the model can be independently reproduced, critically evaluated, and systematically reused across different research contexts. Furthermore, all resources are provided under permissive MIT and CC-BY licences, facilitating broad adoption in both academic and industrial environments and enabling straightforward integration into existing workflows, including commercial applications.

In conclusion, this PBPK digital twin of rapamycin integrates available clinical data into a mechanistic framework that captures key pharmacokinetic processes across dosing regimens and patient populations. The model provides quantitative insight into dose dependency and factors influencing variability in drug action. By providing full open access to the model, this work establishes a transparent and reproducible reference framework that supports independent validation, reuse, and further improvement of future PBPK models of rapamycin and other immunosuppressive drugs.

 doi:10.20944/preprints202605.0328.v1

Author Contributions: Conceptualization, M.J. and M.K.; methodology, M.J. and M.K.; software, M.J. and M.K.; validation, M.J. and M.K.; formal analysis, M.J. and M.K.; data curation, M.J. and M.K.; writing—original draft preparation, M.J. and M.K.; writing—review and editing, M.J. and M.K.; visualization, M.J. and M.K.; supervision, M.K.; project administration, M.K.; funding acquisition, M.K. All authors have read and agreed to the published version of the manuscript.

Funding: M.J. was supported by the Humboldt Internship Program (HIP) 2025. M.K. was supported by the Federal Ministry of Research, Technology and Space (BMFTR, Germany) within ATLAS by grant number 031L0304B and by the German Research Foundation (DFG) by the DFG grant number 436883643 and 465194077.

Data Availability Statement: All curated pharmacokinetic data are publicly available in the PK-DB database (https://pk-db.com). The model and all associated materials (simulation scripts, parameters, and documentation) are publicly available in SBML format under a CC-BY 4.0 license at https://github.com/matthiaskoenig/rapamycin-model [32].

Acknowledgments: The authors declare that the research was conducted in the absence of any commercial or financial relationships that could be construed as a potential conflict of interest. This work was supported by the BMBF-funded de.NBI Cloud within the German Network for Bioinformatics Infrastructure (de.NBI) (031A537B, 031A533A, 031A538A, 031A533B, 031A535A, 031A537C, 031A534A, 031A532B). Created in BioRender. König, M. (2026) https://BioRender.com/6u2rz4i

References

1. Benjamin, D.; Colombi, M.; Moroni, C.; Hall, M.N. Rapamycin Passes the Torch: A New Generation of mTOR Inhibitors. *Nature Reviews. Drug Discovery* **2011**, *10*, 868–880. https://doi.org/10.1038/nrd3531.
2. Basa-Dénes, O.; Angi, R.; Kárpáti, B.; Jordán, T.; Ötvös, Z.; Erdősi, N.; Ujhelyi, A.; Ordasi, B.; Molnár, L.; McDermott, J.; et al. Dose Escalation Study to Assess the Pharmacokinetic Parameters of a Nano-amorphous Oral Sirolimus Formulation in Healthy Volunteers. *European journal of drug metabolism and pharmacokinetics* **2019**, *44*, 777–785. https://doi.org/10.1007/s13318-019-00562-y.
3. Sehgal, S.N.; Baker, H.; Vézina, C. Rapamycin (AY-22,989), a New Antifungal Antibiotic. II. Fermentation, Isolation and Characterization. *The Journal of Antibiotics* **1975**, *28*, 727–732. https://doi.org/10.7164/antibiotics.28.727.
4. Kahan, B.D. Sirolimus: A Comprehensive Review. *Expert opinion on pharmacotherapy* **2001**, *2*, 1903–1917. https://doi.org/10.1517/14656566.2.11.1903.
5. Korth-Bradley, J.M.; Bhattacharya, I.; Matschke, K.; Diehl, A.M.; Longfellow, C.; Gourley, I. Comparative Sirolimus Pharmacokinetics After Single-Dose Administration of Two Prototype 0.5-Mg Tablets in Healthy Volunteers. *Clinical pharmacology in drug development* **2012**, *1*, 52–56. https://doi.org/10.1177/2160763X12438746.
6. Sattler, M.; Guengerich, F.P.; Yun, C.H.; Christians, U.; Sewing, K.F. Cytochrome P-450 3A Enzymes Are Responsible for Biotransformation of FK506 and Rapamycin in Man and Rat. *Drug metabolism and disposition: the biological fate of chemicals* **1992 Sep-Oct**, *20*, 753–761.
7. Mahalati, K.; Kahan, B.D. Clinical Pharmacokinetics of Sirolimus. *Clinical pharmacokinetics* **2001**, *40*, 573–585. https://doi.org/10.2165/00003088-200140080-00002.
8. Leung, L.Y.; Lim, H.K.; Abell, M.W.; Zimmerman, J.J. Pharmacokinetics and Metabolic Disposition of Sirolimus in Healthy Male Volunteers after a Single Oral Dose. *Therapeutic drug monitoring* **2006**, *28*, 51–61. https://doi.org/10.1097/01.ftd.0000179838.33020.34.
9. Candela-Boix, M.R.; Ramón-López, A.; Nalda-Molina, R.; Díaz-González, M.; Márquez-Megías, S.; Más-Serrano, P. Population Pharmacokinetics Models of Sirolimus in Renal Transplant Patients: A Systematic Review. *Farmacia Hospitalaria: Organo Oficial De Expresion Cientifica De La Sociedad Espanola De Farmacia Hospitalaria* **2021**, *45*, 77–83.
10. Hartmanshenn, C.; Scherholz, M.; Androulakis, I.P. Physiologically-Based Pharmacokinetic Models: Approaches for Enabling Personalized Medicine. *Journal of Pharmacokinetics and Pharmacodynamics* **2016**, *43*, 481–504. https://doi.org/10.1007/s10928-016-9492-y.
11. Emoto, C.; Fukuda, T.; Cox, S.; Christians, U.; Vinks, A.A. Development of a Physiologically-Based Pharmacokinetic Model for Sirolimus: Predicting Bioavailability Based on Intestinal CYP3A Content. *CPT: pharmacometrics & systems pharmacology* **2013**, *2*, e59. https://doi.org/10.1038/psp.2013.33.

 doi:10.20944/preprints202605.0328.v1

12. Emoto, C.; Fukuda, T.; Johnson, T.N.; Adams, D.M.; Vinks, A.A. Development of a Pediatric Physiologically Based Pharmacokinetic Model for Sirolimus: Applying Principles of Growth and Maturation in Neonates and Infants. *CPT: pharmacometrics & systems pharmacology* **2015**, *4*, e17. https://doi.org/10.1002/psp4.17.
13. Emoto, C.; Fukuda, T.; Venkatasubramanian, R.; Vinks, A.A. The Impact of CYP3A5*3 Polymorphism on Sirolimus Pharmacokinetics: Insights from Predictions with a Physiologically-Based Pharmacokinetic Model. *British journal of clinical pharmacology* **2015**, *80*, 1438–1446. https://doi.org/10.1111/bcp.12743.
14. Domínguez-Romero, E.; Mazurenko, S.; Scheringer, M.; Martins Dos Santos, V.A.P.; Evelo, C.T.; Anton, M.; Hancock, J.M.; Županič, A.; Suarez-Diez, M. Making PBPK Models More Reproducible in Practice. *Briefings in Bioinformatics* **2024**, *25*, bbae569. https://doi.org/10.1093/bib/bbae569.
15. Tiwari, K.; Kananathan, S.; Roberts, M.G.; Meyer, J.P.; Sharif Shohan, M.U.; Xavier, A.; Maire, M.; Zyoud, A.; Men, J.; Ng, S.; et al. Reproducibility in Systems Biology Modelling. *Molecular Systems Biology* **2021**, *17*, e9982. https://doi.org/10.15252/msb.20209982.
16. Wilkinson, M.D.; Dumontier, M.; Aalbersberg, I.J.J.; Appleton, G.; Axton, M.; Baak, A.; Blomberg, N.; Boiten, J.W.; da Silva Santos, L.B.; Bourne, P.E.; et al. The FAIR Guiding Principles for Scientific Data Management and Stewardship. *Scientific Data* **2016**, *3*, 160018. https://doi.org/10.1038/sdata.2016.18.
17. Balaur, I.; Nickerson, D.P.; Welter, D.; Wodke, J.A.; Ancien, F.; Gebhardt, T.; Grouès, V.; Hermjakob, H.; König, M.; Radde, N.; et al. FAIRification of Computational Models in Biology, 2025. https://doi.org/10.1101/2025.03.21.644517.
18. Grzegorzewski, J.; Brandhorst, J.; Green, K.; Eleftheriadou, D.; Duport, Y.; Barthorscht, F.; Köller, A.; Ke, D.Y.J.; De Angelis, S.; König, M. PK-DB: Pharmacokinetics Database for Individualized and Stratified Computational Modeling. *Nucleic Acids Research* **2021**, *49*, D1358–D1364. https://doi.org/10.1093/nar/gkaa990.
19. Rohatgi, A. WebPlotDigitizer, 2024.
20. König, M. Sbmlutils: Python Utilities for SBML. Zenodo, 2026. https://doi.org/10.5281/ZENODO.18207772.
21. König, M. Sbmlsim: SBML Simulation Made Easy. Zenodo, 2026. https://doi.org/10.5281/ZENODO.18452043.
22. Welsh, C.; Xu, J.; Smith, L.; König, M.; Choi, K.; Sauro, H.M. libRoadRunner 2.0: A High Performance SBML Simulation and Analysis Library. *Bioinformatics* **2023**, *39*, btac770. https://doi.org/10.1093/bioinformatics/btac770.
23. Somogyi, E.T.; Bouteiller, J.M.; Glazier, J.A.; König, M.; Medley, J.K.; Swat, M.H.; Sauro, H.M. libRoadRunner: A High Performance SBML Simulation and Analysis Library. *Bioinformatics* **2015**, *31*, 3315–3321. https://doi.org/10.1093/bioinformatics/btv363.
24. König, M.; Dräger, A.; Holzhütter, H.G. CySBML: A Cytoscape Plugin for SBML. *Bioinformatics* **2012**, *28*, 2402–2403. https://doi.org/10.1093/bioinformatics/bts432.
25. Jones, H.; Rowland-Yeo, K. Basic Concepts in Physiologically Based Pharmacokinetic Modeling in Drug Discovery and Development. *CPT: Pharmacometrics & Systems Pharmacology* **2013**, *2*, 63. https://doi.org/10.1038/psp.2013.41.
26. Levin, A.; Stevens, P.E. Summary of KDIGO 2012 CKD Guideline: Behind the Scenes, Need for Guidance, and a Framework for Moving Forward. *Kidney International* **2014**, *85*, 49–61. https://doi.org/10.1038/ki.2013.444.
27. Stevens, P.E.; Ahmed, S.B.; Carrero, J.J.; Foster, B.; Francis, A.; Hall, R.K.; Herrington, W.G.; Hill, G.; Inker, L.A.; Kazancıoğlu, R.; et al. KDIGO 2024 Clinical Practice Guideline for the Evaluation and Management of Chronic Kidney Disease. *Kidney International* **2024**, *105*, S117–S314. https://doi.org/10.1016/j.kint.2023.10.018.
28. Child, C.G.; Turcotte, J.G. Surgery and Portal Hypertension. *Major Problems in Clinical Surgery* **1964**, *1*, 1–85.
29. Pugh, R.N.H.; Murray-Lyon, I.M.; Dawson, J.L.; Pietroni, M.C.; Williams, R. Transection of the Oesophagus for Bleeding Oesophageal Varices. *British Journal of Surgery* **1973**, *60*, 646–649. https://doi.org/10.1002/bjs.1800600817.
30. Köller, A.; Grzegorzewski, J.; König, M. Physiologically Based Modeling of the Effect of Physiological and Anthropometric Variability on Indocyanine Green Based Liver Function Tests. *Frontiers in Physiology* **2021**, *12*, 757293. https://doi.org/10.3389/fphys.2021.757293.
31. Köller, A.; Grzegorzewski, J.; Tautenhahn, H.M.; König, M. Prediction of Survival After Partial Hepatectomy Using a Physiologically Based Pharmacokinetic Model of Indocyanine Green Liver Function Tests. *Frontiers in Physiology* **2021**, *12*, 730418. https://doi.org/10.3389/fphys.2021.730418.
32. Jesionek, M.; König, M. Physiologically Based Pharmacokinetic (PBPK) Model of Rapamycin. Zenodo, 2026. https://doi.org/10.5281/zenodo.20036174.

 doi:10.20944/preprints202605.0328.v1

33. Brattström, C.; Säwe, J.; Jansson, B.; Lönnebo, A.; Nordin, J.; Zimmerman, J.J.; Burke, J.T.; Groth, C.G. Pharmacokinetics and Safety of Single Oral Doses of Sirolimus (Rapamycin) in Healthy Male Volunteers. *Therapeutic drug monitoring* **2000**, *22*, 537–544. https://doi.org/10.1097/00007691-200010000-00006.
34. Zimmerman, J.J.; Kahan, B.D. Pharmacokinetics of Sirolimus in Stable Renal Transplant Patients after Multiple Oral Dose Administration. *Journal of clinical pharmacology* **1997**, *37*, 405–415. https://doi.org/10.1002/j.1552-4604.1997.tb04318.x.
35. Leelahavanichkul, A.; Areepium, N.; Vadcharavivad, S.; Praditpornsilpa, K.; Avihingsanon, Y.; Karnjanabuchmd, T.; Eiam-Ong, S.; Tungsanga, K. Pharmacokinetics of Sirolimus in Thai Healthy Volunteers. *Journal of the Medical Association of Thailand = Chotmaihet thangphaet* **2005**, *88 Suppl 4*, S157–162.
36. Kelly, P.A.; Napoli, K.; Kahan, B.D. Conversion from Liquid to Solid Rapamycin Formulations in Stable Renal Allograft Transplant Recipients. *Biopharmaceutics & drug disposition* **1999**, *20*, 249–253. https://doi.org/10.1002/(sici)1099-081x(199907)20:5<249::aid-bdd181>3.0.co;2-9.
37. Rogers, C.C.; Alloway, R.R.; Alexander, J.W.; Cardi, M.; Trofe, J.; Vinks, A.A. Pharmacokinetics of Mycophenolic Acid, Tacrolimus and Sirolimus after Gastric Bypass Surgery in End-Stage Renal Disease and Transplant Patients: A Pilot Study. *Clinical transplantation* **2008**, *22*, 281–291. https://doi.org/10.1111/j.1399-0012.2007.00783.x.
38. Zimmerman, J.J.; Patat, A.; Parks, V.; Moirand, R.; Matschke, K. Pharmacokinetics of Sirolimus (Rapamycin) in Subjects with Severe Hepatic Impairment. *Journal of clinical pharmacology* **2008**, *48*, 285–292. https://doi.org/10.1177/0091270007312902.
39. Renders, L.; Frisman, M.; Ufer, M.; Mosyagin, I.; Haenisch, S.; Ott, U.; Caliebe, A.; Dechant, M.; Braun, F.; Kunzendorf, U.; et al. CYP3A5 Genotype Markedly Influences the Pharmacokinetics of Tacrolimus and Sirolimus in Kidney Transplant Recipients. *Clinical pharmacology and therapeutics* **2007**, *81*, 228–234. https://doi.org/10.1038/sj.clpt.6100039.
40. Zhang, J.; Dai, Y.; Liu, Z.; Zhang, M.; Li, C.; Chen, D.; Song, H. Effect of CYP3A4 and CYP3A5 Genetic Polymorphisms on the Pharmacokinetics of Sirolimus in Healthy Chinese Volunteers. *Therapeutic drug monitoring* **2017**, *39*, 406–411. https://doi.org/10.1097/FTD.0000000000000415.
41. Zha, J.; Jiang, Q.; Yao, B.B.; Cohen, D.E.; Carter, D.C.; Menon, R.M. Effects of a Ritonavir-Containing Regimen on the Pharmacokinetics of Sirolimus or Everolimus in Healthy Adult Subjects. *Pharmacology research & perspectives* **2022**, *10*, e01024. https://doi.org/10.1002/prp2.1024.
42. Böttiger, Y.; Säwe, J.; Brattström, C.; Tollemar, J.; Burke, J.T.; Häss, G.; Zimmerman, J.J. Pharmacokinetic Interaction between Single Oral Doses of Diltiazem and Sirolimus in Healthy Volunteers. *Clinical pharmacology and therapeutics* **2001**, *69*, 32–40. https://doi.org/10.1067/mcp.2001.112513.
43. Tortorici, M.A.; Matschke, K.; Korth-Bradley, J.M.; DiLea, C.; Lasseter, K.C. The Effect of Rifampin on the Pharmacokinetics of Sirolimus in Healthy Volunteers. *Clinical pharmacology in drug development* **2014**, *3*, 51–56. https://doi.org/10.1002/cpdd.40.
44. Tortorici, M.A.; Parks, V.; Matschke, K.; Korth-Bradley, J.; Patat, A. The Evaluation of Potential Pharmacokinetic Interaction between Sirolimus and Tacrolimus in Healthy Volunteers. *European journal of clinical pharmacology* **2013**, *69*, 835–842. https://doi.org/10.1007/s00228-012-1407-2.
45. Zimmerman, J.J.; Harper, D.; Getsy, J.; Jusko, W.J. Pharmacokinetic Interactions between Sirolimus and Microemulsion Cyclosporine When Orally Administered Jointly and 4 Hours Apart in Healthy Volunteers. *Journal of clinical pharmacology* **2003**, *43*, 1168–1176. https://doi.org/10.1177/0091270003257227.
46. Wang, H.F.; Qiu, F.; Wu, X.; Fang, J.; Crownover, P.; Korth-Bradley, J.; Schulman, S. Steady-State Pharmacokinetics of Sirolimus in Stable Adult Chinese Renal Transplant Patients. *Clinical pharmacology in drug development* **2014**, *3*, 235–241. https://doi.org/10.1002/cpdd.96.
47. Zimmerman, J.J.; Lasseter, K.C.; Lim, H.K.; Harper, D.; Dilzer, S.C.; Parker, V.; Matschke, K. Pharmacokinetics of Sirolimus (Rapamycin) in Subjects with Mild to Moderate Hepatic Impairment. *Journal of clinical pharmacology* **2005**, *45*, 1368–1372. https://doi.org/10.1177/0091270005281350.
48. Zimmerman, J.J.; Ferron, G.M.; Lim, H.K.; Parker, V. The Effect of a High-Fat Meal on the Oral Bioavailability of the Immunosuppressant Sirolimus (Rapamycin). *Journal of clinical pharmacology* **1999**, *39*, 1155–1161.